Nuclear Instruments and Methods in Physics Research B 342 (2015) 234–239

Contents lists available at ScienceDirect

Nuclear Instruments and Methods in Physics Research B

journal homepage: www.elsevier.com/locate/nimb

# Sputtering of a metal nanofoam by Au ions

Christian Anders [a], Eduardo M. Bringa [b,c], Herbert M. Urbassek [a,*]

[a] Physics Department and Research Center OPTIMAS, University Kaiserslautern, Erwin-Schrödinger-Straße, D-67663 Kaiserslautern, Germany
[b] CONICET, Mendoza 5500, Argentina
[c] Instituto de Ciencias Básicas, Universidad Nacional de Cuyo, Mendoza 5500, Argentina

ARTICLE INFO

*Article history:*
Received 9 August 2014
Received in revised form 2 October 2014
Accepted 6 October 2014

*Keywords:*
Sputtering
Molecular dynamics
Porosity
Spikes

ABSTRACT

Porous materials, such as nanofoams, may react differently to irradiation than compact targets. This is caused by the influence of the cavities on the evolution of collision cascades, but also by the differing heat conduction which affects the spike phase. Using molecular dynamics simulation we study the sputtering of a Au nanofoam by 10 keV Au projectiles, and compare to the sputtering of a compact Au target. These bombardment conditions lead to a strong contribution of spikes to the sputtering process. We find the foam to sputter considerably less than the compact target; the open structure of the foam prevents the build-up of strong collision spike regions at the surface, which are the major source of sputtering in the compact target. Also emission takes a longer time scale in the foam, as particles need to travel longer pathways to be emitted. On the other hand, the molten phase is more extended in the foam and also exists for a longer time; this is caused by the reduced heat conductivity in this material.



## 1. Introduction

The recent availability of nanoporous materials such as metal foams started investigations on their potential uses. In the field of ion irradiation the response of foams to irradiation and their differences and possible advantages to traditional compact solids were investigated [1–4]. A prime finding of these investigations was that foams are radiation resistant because their high surface-to-volume ratio increases the annealing of radiation-induced defects. Nanoporous materials are also ubiquitous in the space environment, such as dust grain agglomerates, regolith surfaces of moons or amorphous ice surfaces. Studies of the sputtering of regolith showed a considerable decrease if compared to the compact material [5].

While these studies focused on the effects of radiation damage creation and annihilation, also the effects on the sputtering received attention. In particular high-energy irradiation was investigated, where the particle penetration depth (range $R$) is considerably larger than the typical filament diameter ($D$) of the foam. Under such circumstances it was found that the foam sputters similarly as the compact solid. It was argued that this is due to the fact that while the nominal density of the foam is smaller, the escape depth of emitted particles is larger, and these two effects tend to cancel.

Linear collision cascade sputtering has long been known to be independent of the atom number density $n$ of the irradiated material [6]. In porous media this argument breaks down since the material is inhomogeneous. In this article we wish to explore the consequences of this breakdown.

Let us call the porosity of the sample $p$. If the ion range $R$ is large compared to the filament diameter $D$, the sample looks homogeneous with a reduced density $pn$ on the scale of the ion range. Hence energy deposition at the surface is reduced by a factor $p$. On the other hand, the atom escape length is increased by the reduced density by a factor $1/p$; in total we expect

$$Y(p) = Y(p=1), \quad R \gg D. \tag{1}$$

This expectation has been confirmed by simulations of high-energy ion impact creating a hot cylindrical track, where $R \gg D$ [1].

On the other hand, when ions have ranges $R \ll D$, they encounter locally compact material with probability $p$. If they hit a hole at the surface (with probability $1-p$), in the simplest model they do not contribute to sputtering, since the collision cascade will happen far down in the porous material and the particles emitted there have a high chance of being redeposited. Hence

$$Y(p) = pY(p=1), \quad R \ll D. \tag{2}$$

In a more refined treatment, the buried impacts will also contribute to sputtering, in particular if the sticking probability is low, increasing $Y(p)$. The influence of the geometry of the porous target on the sputtering is a complex issue, and has been addressed in particular with the help of Monte Carlo simulations [4,5].

* Corresponding author.
*E-mail address:* urbassek@rhrk.uni-kl.de (H.M. Urbassek).
*URL:* http://www.physik.uni-kl.de/urbassek/.

http://dx.doi.org/10.1016/j.nimb.2014.10.005
0168-583X/

In this paper we explore the effects of target porosity on sputtering in the so-called spike regime of sputtering. In contrast to linear collision-cascade sputtering, this regime is characterized by a near-surface zone where the projectile deposited a large amount of energy [7,8]. The resulting high energy density leads to abundant sputtering which is often connected with crater formation at the surface. We study this sputtering regime by considering the concrete case of a 10 keV Au ion impacting on a Au nanofoam.

## 2. Method

We use the parallelized molecular dynamics simulation package LAMMPS [9] for our study.

The Au target has been constructed from a prototype generated as in Refs. [10,11] by a phase-field model simulating the spinodal decomposition of a binary alloy. The structure has a porosity of $p = 0.5$ and an average filament diameter of $D = 3$ nm. In order to contain the collision cascades created, this structure is repeated 9 times to obtain the final foam target. It has a total number of $1.5 \times 10^6$ atoms and extends over $(367\ \text{Å})^3$.

For comparison, also a compact Au target is studied. Here the size could be reduced since cascades have smaller extensions. The total number of atoms amounts to $0.52 \times 10^6$, and the target extends over $(204\ \text{Å})^3$.

Both the porous and the compact target have a (100) surface. The targets have been relaxed to 0 K before the start of the simulations. At the lateral and bottom sides of the simulation targets, we employ damped boundary conditions in order to mimic energy dissipation to the surrounding target material, while at the top surfaces free boundary conditions are applied.

The targets are bombarded by 10 keV atoms. The individual impacts differ from each other by the exact location of the impact point and by the impact azimuth. The impact points are varied inside the irreducible triangle of the fcc (100) surface. All impact trajectories have an inclination of 7° to the surface normal; the impact azimuth is aligned in ⟨100⟩ and ⟨110⟩ directions. The small tilt of the incidence direction by 7° is used to avoid channeling of the projectile along the [100] direction. For each of the targets, 33 impacts have been simulated. We follow each simulation until a time of 100 ps after impact.

A many-body potential, which reproduces the melting temperature of Au, $T_m = 1338$ K, has been employed [12–14]. It has a cutoff of $r_c = 6.2$ Å. At these low impact energies, the influence of electronic stopping is only minor; therefore no electronic stopping has been applied. The influence of the electron–phonon coupling on the quenching of the spike generated by the impact may be important [15]. However, the electronic heat conduction in foamy structures is changed with respect to that in compact materials [16,17]; this makes the correct inclusion of electronic effects during the spike phase a complex task. We therefore omit electronic effects altogether.

The sputter yield is determined by using Stoddard's clustering algorithm [18]. It groups all Au atoms in disjoint sets such that atoms into any such set have zero interaction energy with the atoms of the other sets, but non-zero interaction with at least one other atom of the same set. The atoms in the largest set still belong to the target; all other atoms have lost contact with the target and are considered sputtered.

We determine the local temperature in the irradiated target by calculating the kinetic energy around each atom in a sphere with radius $r_c$ and averaging it [19]. This algorithm is also used to determine the 'molten atoms', i.e., the atoms whose local temperature is above the melting point of Au, $T_m = 1338$ K.

## 3. Results and discussion

Fig. 1 shows the changes induced by particle impact into the foam structure for an exemplary event. The irradiation changes the foam structure locally, but the global characteristics are conserved. In this particular example one pore widens and a filament thickens. Note that the foam neither compactifies nor dissolves.

### 3.1. Sputter yields

We obtain a sputter yield of $80 \pm 19$ in the compact target, and of $15 \pm 5$ in the foam target. Here the second number gives the average error of the mean value taken over the 33 impact events.

In Fig. 2 three impact events into the foam are shown and can be compared to impacts into the compact target in Fig. 3. In each case we show the size of the molten zone at the time of largest extension. The length scales of the figures are identical to allow comparison. Impacts into the compact target, Fig. 3, lead to localized melt zones; these are the spikes that are generated by the ion impact. The form of the spikes varies from impact to impact. If the spike is close to the surface and has a large cross-sectional area at the surface, it gives rise to abundant sputtering. If the spike is, however, buried in the target or has an elongated form with small intersection area with the surface, the sputter yield is low.

Impact into the foam may result in quite different spike shapes and locations. In Fig. 2(a), the ion penetrates deeply through a hole

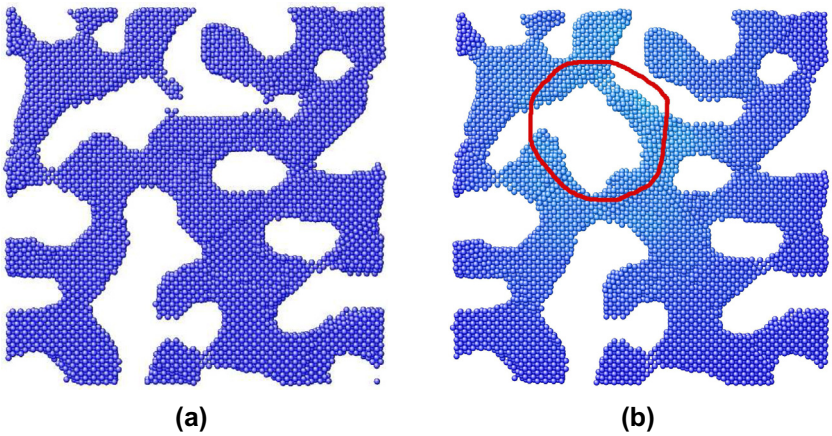


**Fig. 1.** Cross-sectional view (0.6 nm deep) of the irradiated foam target (a) before and (b) at 82 ps after impact. The region where filament changes are most pronounced is highlighted. Only a 20-nm wide part of the total structure is shown. Impact from the top. Colors indicate remaining temperature in the target; it is on average 83 K with a maximum of 394 K. (For interpretation of the references to color in this figure legend, the reader is referred to the web version of this article.)

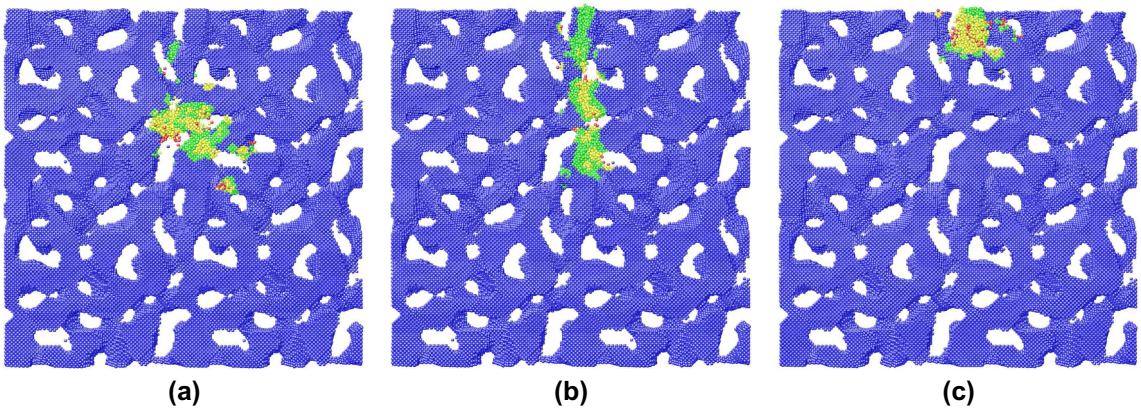


**Fig. 2.** Cross-sectional views of the irradiated foam targets for several impact events at the time of maximum melt extension. The foam targets have a width of 40 nm. Color codes local temperature: blue: solid phase, $T < T_m$; green: molten phase, $T_m < T < T_v$; yellow: boiling, $T_v < T < T_c$; red: supercritical, $T > T_c$. $T_m = 1337$ K, $T_v = 3081$ K, $T_c = 7400$ K [20]. The three events shown differ in their sputter yields: (a) $Y = 1$; (b) $Y = 9$; (c) $Y = 123$. (For interpretation of the references to color in this figure legend, the reader is referred to the web version of this article.)

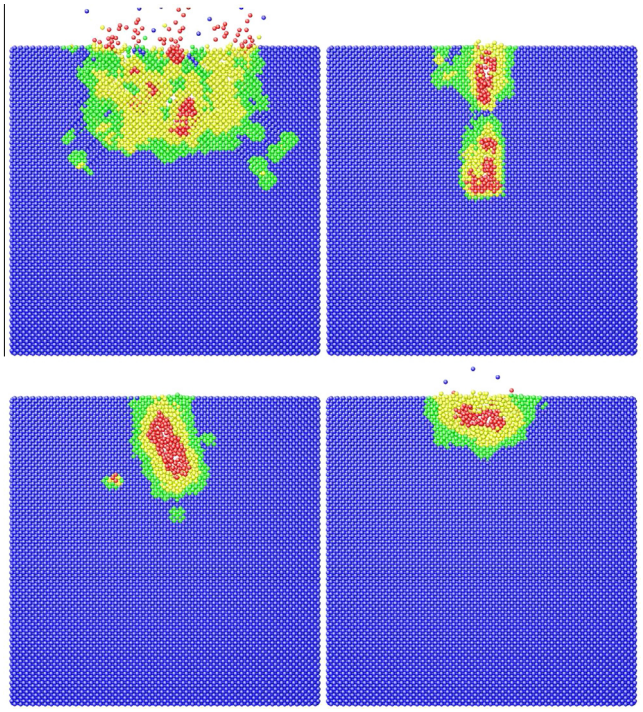

**Fig. 3.** Cross-sectional views of the irradiated compact targets for several impact events at the time of maximum melt extension. The target width shown amounts to 20 nm. Color codes local temperature as in Fig. 2. The four events shown differ in their sputter yields. In clockwise direction starting from the upper left these amount to: $Y = 116; Y = 47; Y = 343; Y = 12$. (For interpretation of the references to color in this figure legend, the reader is referred to the web version of this article.)

close to the surface. The projectile energy is deposited deep in the target, hence little emission results. In Fig. 2(b), the projectile also penetrates deeply due to the foamy structure; however, a small amount of energy is deposited at the target surface; hence moderate sputtering occurs. Finally, in Fig. 2(c) the projectile creates a collision cascade in a filament immediately at the surface; this leads to a sputter yield comparable to that in the compact target.

These figures demonstrate that not only the position of impact on the foam but also the topology of the foam beneath the impact point are important parameters to determine the path of the projectile, and hence energy deposition and sputtering.

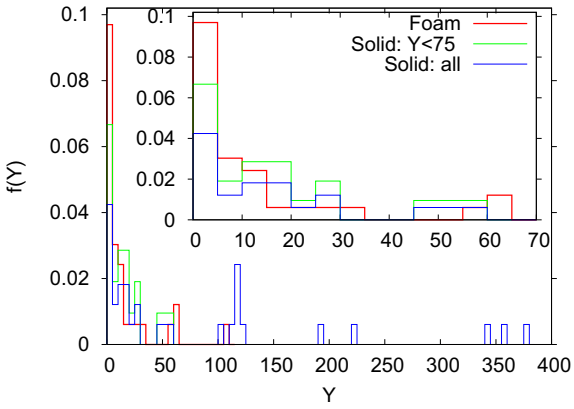


**Fig. 4.** Yield statistics, i.e., normalized number of impacts which give rise to sputter yield $Y$. The inset shows a zoom for small-yield events.

Fig. 4 quantifies these considerations by showing the yield statistics for the two targets. Abundant sputter events for the foam are rare. In contrast, the yield statistics for the compact target is very wide; the maximum sputter yield amounts to 337 atoms. Clearly the large sputter yields are connected to spike sputtering; we therefore form a sub-group of the compact sputter events by including only those impacts in which the yield is below $Y < 75$ (*moderate events*). As Fig. 4 demonstrates, the statistics of these moderate events is quite similar to those of the foam. In the compact target, 21 events showed a sputter yield $< 75$ with an average of $16 \pm 4$. We shall use these moderate events also in our further discussion for comparing compact-target and foam yields.

### 3.2. Characteristics of emission

Fig. 5 shows the time evolution of the irradiation by concentrating on two quantities: (a) the number $N_{\mathrm{melt}}$ of atoms whose local temperature is above the melting temperature ('molten atoms'), and (b) the sputter yield. While $N_{\mathrm{melt}}$ characterizes the energy sharing and cascade thermalization in the material, and thus the spike volume, $Y(t)$ is of immediate relevance to emission.

Energy sharing in the foam evolves with a considerably different dynamics than in the compact target, see Fig. 5(a). In the compact target, the number of molten atoms reaches its maximum at around 0.34 ps. At this time the spike developing after the linear collision-cascade phase has reached its maximum extension

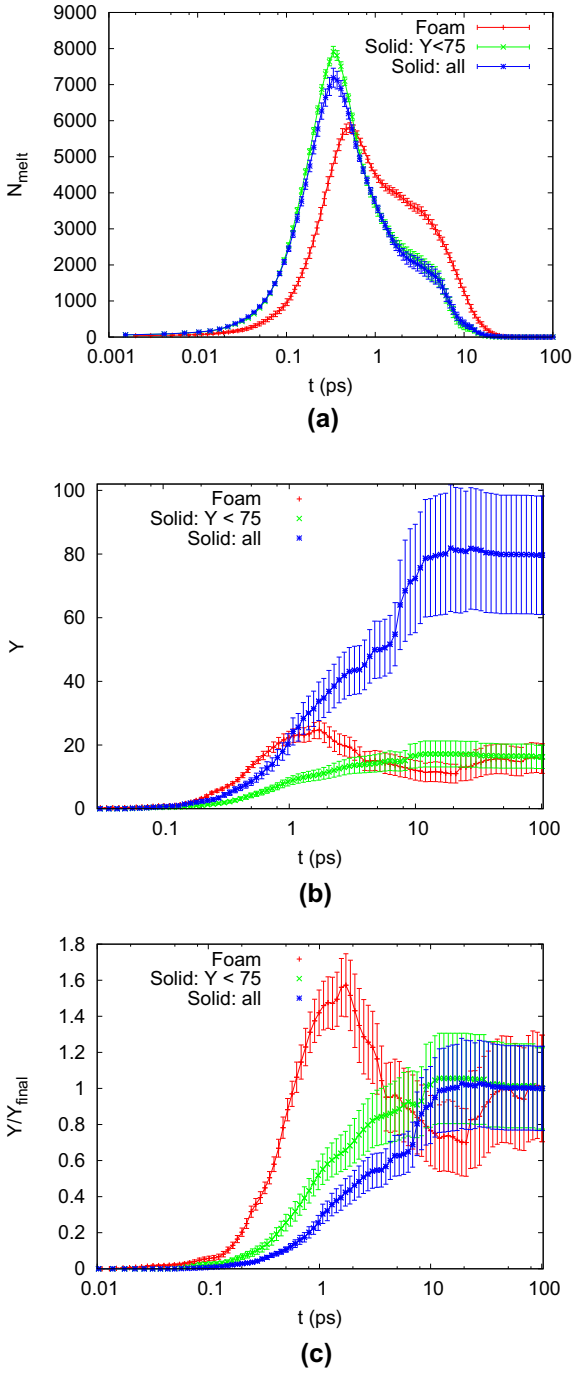


**Fig. 5.** Temporal evolution of (a) the number of atoms with $T > T_m$, and (b) the sputter yield. (c) shows the data of (b) scaled to the final yield at the end of the simulation.

(7200 atoms); thereafter the spike volume shrinks due to heat conduction to the surroundings. In the foam, two differences show up: (i) the spike volume is smaller (5800 atoms) and its maximum is reached somewhat later, at 0.52 ps. (ii) The spike burns longer; this means that the heat is transported less efficiently away. The reduced heat conduction is caused by the decreased thermal contact within the porous foam structure.

The time evolution of the sputter emission in the foam is interesting in that it shows a maximum at 1.7 ps and then decreases again. This non-monotonic behavior is caused by re-deposition; atoms which got sputtered from the interior surfaces of the foam

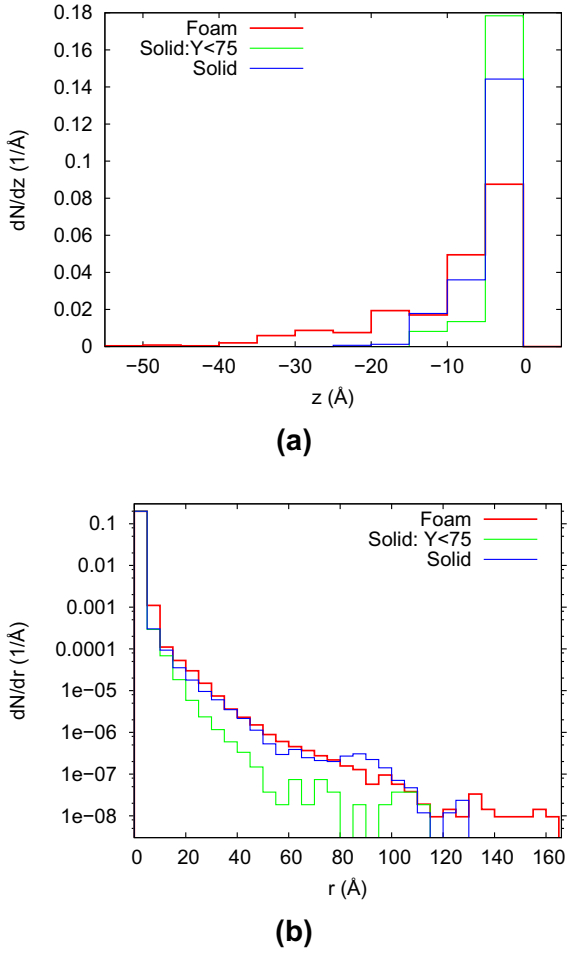


**Fig. 6.** Distribution of (a) depth of origin of sputtered particles, and (b) of displacement of particles from their initial position.

get redeposited on the interior walls. Interestingly, however, the initial evolution ($t \lesssim 1$ ps) of sputtered particles is quite similar to that of the compact solid.

The yields of the compact solid saturate after around 20 ps; this proves that our simulation time of 100 ps is sufficient to capture the relevant sputtering physics. Note that it is known that emitted clusters are hot and will partly break up on time scales of μs [21]; some fragments may then be re-deposited on the surface thus decreasing the final sputter yield [22]. The evolution of the moderate events proceeds on the same time scale as that of all compact-solid sputtering events. When scaling the time evolution data of all and moderate compact-solid sputtering events to the final yield, Fig. 5(c), only small differences remain. The emission of moderate events is more concentrated at early times, while late emission contributes more to the high-yield events.

The depth of origin of sputtered particles is plotted in Fig. 6(a). Linear collision-cascade sputtering would show maximum emission from the 2 first layers for (100) crystals, as molecular-dynamics simulations show [23]. In our case, the compact target shows maximum emission from the first 5 Å; 72% of all emitted particles originate from this depth. The remaining sputtered atoms originate from depths extending up to 20 Å. The emission characteristics of moderate events shows a higher percentage of emission from near-surface regions; 90% originate from the uppermost 5 Å. This demonstrates that the melt pool created by pronounced spike events allows particles to be sputtered from larger depths. In the foam only 44% of the atoms originate from the first 5 Å below

the surface. Emission extends to depths of 40 Å with a non-negligible probability, and a few atoms even come from larger depths, up to 80 Å below the surface. These are particles which have been emitted from buried filaments of the foam structure.

The open structure of the porous target lets us assume that recoil atoms are more easily relocated in the foam target than in the compact target. We measure the distance $r$ by which atoms have been relocated from their initial position in the material and display the probability distribution of such relocations in Fig. 6(b). Sputtered atoms have not been included in this plot. The figure shows an astonishing similarity of the relocation probability for the foam and the compact target. The small peak in the compact target at $r \cong 80$ Å stems from relocations in the melt zone. A detailed analysis reveals that these are due to atoms transported from the interior of the melt pool to the crater rim. We argue that long-range transport in the compact target is possible due to the high atom mobility in the melt zone created. This is proven by comparing the data to those for the set of moderate-sputtering events; here indeed the relocation probability quickly decreases with distance. In the foam target the porous structure allows for large-range relocations. We note that in the linear collision-cascade regime of ion irradiation considerably stronger differences between the relocations in a compact and a foam target are observed [1].

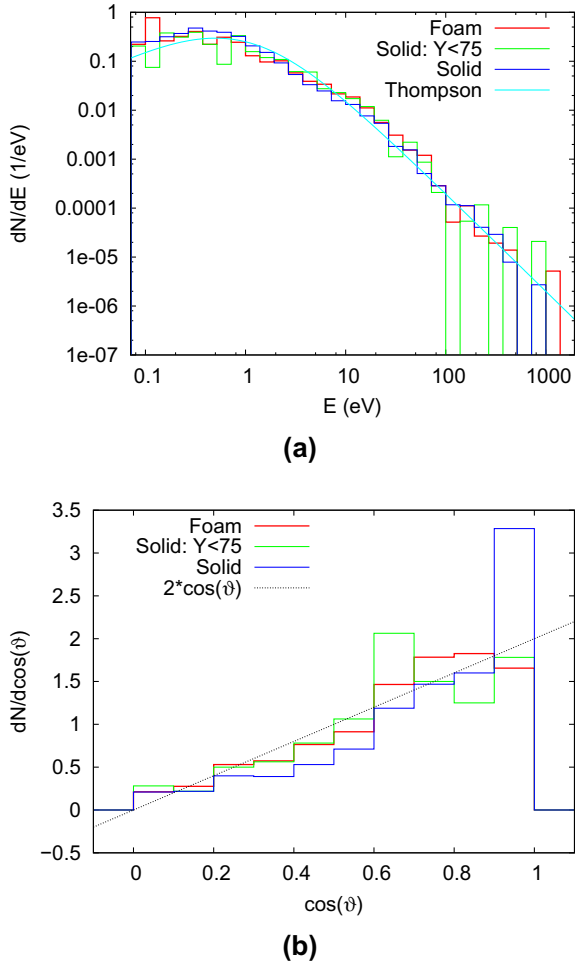


**Fig. 7.** (a) Normalized energy distribution of sputtered particles. A Thompson distribution characteristic of linear collision-cascade sputtering, Eq. (3), has been included for reference. (b) Normalized distribution of the emission angle (with respect to the surface normal) of sputtered particles. A cosine distribution has been added for reference.

The energy distribution of emitted particles, Fig. 7(a), shows little differences between the compact target and the foam. A Thompson distribution [7,24] has been added, which reads when normalized

$$f(E) = \frac{2EU}{(E+U)^3}, \tag{3}$$

and describes linear collision-cascade sputtering well. In a collision cascade, a value of $U = 3.79$ eV for the surface binding energy applies; this would give a maximum of the energy spectrum at $U/2 = 1.9$ eV which is evidently at too large energies. We therefore chose $U = 1$ eV in this plot; this reproduces the low-energy side of the spectrum quite nicely. This effective reduction of the binding energy can be associated with thermal ejection processes [25–28]. The energy distributions of both the foam and the compact target follow this reference distribution well. This shows that the energy distribution cannot be used to distinguish particle emission from the 2 targets.

The angular distributions of sputtered particles, Fig. 7(b), follow well a cosine distribution. Emission from the compact solid features a peak at normal emission; this indicates the formation of a jet emitted along the surface normal. Note that it is not present for the moderate-event set; this shows that the emission jet stems from near-surface spikes which emit atoms preferentially in the direction of the surface normal, as seen in Fig. 3.

## 4. Conclusions

Sputtering a metal nanofoam in the spike regime leads to a considerably smaller sputter yield than for a compact target. This is in strong contrast to linear collision-cascade sputtering where the sputter yield is affected only little, at least as long as the projectile range is large compared to the filament diameter of the foam.

We find that the strong collision spikes which lead to abundant sputtering for the compact target are suppressed in the foam. Even in cases where the ion delivers a large amount of energy close to the surface the induced spike volume is restricted to a single filament, and thus effectively prohibits the abundant sputter events. The formation of an emission jet in the direction of the target normal – a typical feature of spike sputtering – is missing in foams.

Ion irradiation of a foam target leads to emission from deep inside the material and a large relocation probability of atoms inside the material. In consequence, sputtering lasts longer in the foam target. In addition, we observe 'interior' sputtering of particles from the surfaces of voids, which are later re-deposited at other walls.

When subtracting the abundant spike events – defined here as those with an emission yield larger than the average value – from the compact-target sputtering data, the remaining events show a strong resemblance with the foam sputter data: angular emission distribution, time evolution of the sputter yield.

Our results for a structure often assumed as a collection of connected nanowires contrasts sharply with the huge sputter-yield enhancement found for the sputtering of a single nanorod [29], pointing to the need for integrative studies of nanofoams [30].

## Acknowledgments

We thank Diana Farkas for providing the porous sample. E.M.B. would like to thank funding from PICT2009–0092 and a SeCTyP grant. Part of the work of EMB was financed by MINECO (Spain) under project MAT2012-38541-C02-01.

## References

[1] J.F. Rodriguez-Nieva, E.M. Bringa, T.A. Cassidy, R.E. Johnson, A. Caro, M. Fama, M.J. Loeffler, R.A. Baragiola, D. Farkas, Astrophys. J. Lett. 743 (2011) L5.

[2] E.M. Bringa, J.D. Monk, A. Caro, A. Misra, L. Zepeda-Ruiz, M. Duchaineau, F. Abraham, M. Nastasi, S.T. Picraux, Y.Q. Wang, et al., Nano Lett. 12 (2012) 3351.
[3] E.G. Fu, M. Caro, L.A. Zepeda-Ruiz, Y. Wang, K. Baldwin, E. Bringa, M. Nastasi, A. Caro, Appl. Phys. Lett. 101 (2012) 191607.
[4] J.F. Rodriguez-Nieva, E.M. Bringa, Nucl. Instr. Meth. B 304 (2013) 23.
[5] T.A. Cassidy, R.E. Johnson, Icarus 176 (2005) 499.
[6] P. Sigmund, Thin Solid Films 520 (2012) 6031.
[7] P. Sigmund, in: R. Behrisch (Ed.), Sputtering by Particle Bombardment I, Springer, Berlin, 1981, p. 9.
[8] T.J. Colla, R. Aderjan, R. Kissel, H.M. Urbassek, Phys. Rev. B 62 (2000) 8487.
[9] S. Plimpton, J. Comput. Phys. 117 (1995) 1. http://lammps.sandia.gov/.
[10] D.A. Crowson, D. Farkas, S.G. Corcoran, Scr. Mater. 56 (2007) 919.
[11] D.A. Crowson, D. Farkas, S.G. Corcoran, Scr. Mater. 61 (2009) 497.
[12] T.J. Colla, H.M. Urbassek, Nucl. Instr. Meth. B 164–165 (2000) 687.
[13] S. Zimmermann, H.M. Urbassek, Nucl. Instr. Meth. B 228 (2005) 75.
[14] S. Zimmermann, H.M. Urbassek, Nucl. Instr. Meth. B 255 (2007) 208.
[15] L. Sandoval, H.M. Urbassek, Phys. Rev. B 79 (2009) 144115.
[16] P.E. Hopkins, P.M. Norris, L.M. Phinney, S.A. Policastro, R.G. Kelly, J. Nanomater. 2008 (2008) 418050.
[17] P.E. Hopkins, J.R. Serrano, L.M. Phinney, H. Li, A. Misra, J. Appl. Phys. 109 (2011) 013524.
[18] S.D. Stoddard, J. Comput. Phys. 27 (1978) 291.
[19] T.J. Colla, H.M. Urbassek, Radiat. Eff. Defects Solids 142 (1997) 439.
[20] K. Boboridis, G. Pottlacher, H. Jäger, Int. J. Thermophys. 20 (1999) 1289.
[21] A. Wucher, B.J. Garrison, Phys. Rev. B 46 (1992) 4855.
[22] K.O.E. Henriksson, K. Nordlund, J. Keinonen, Phys. Rev. B 71 (2005) 014117.
[23] M.H. Shapiro, E. Trovato, T.A. Tombrello, Nucl. Instr. Meth. B 180 (2001) 58.
[24] M.W. Thompson, Philos. Mag. 18 (1968) 377.
[25] R.A. Haring, R. Pedrys, A. Haring, A.E. de Vries, Nucl. Instr. Meth. B 4 (1984) 40. erratum B6 (1985) 585.
[26] H.M. Urbassek, J. Michl, Nucl. Instr. Meth. B 22 (1987) 480.
[27] R. Pedrys, Nucl. Instr. Meth. B 48 (1990) 525.
[28] E.M. Bringa, R.E. Johnson, Phys. Rev. Lett. 88 (2002) 165501.
[29] G. Greaves, J.A. Hinks, P. Busby, N.J. Mellors, A. Ilinov, A. Kuronen, K. Nordlund, S.E. Donnelly, Phys. Rev. Lett. 111 (2013) 065504.
[30] M. Caro, W.M. Mook, E.G. Fu, Y.Q. Wang, C. Sheehan, E. Martinez, J.K. Baldwin, A. Caro, Appl. Phys. Lett. 104 (2014) 233109.